NEUROSCIENCE

Dynamic Fas signaling network regulates neural stem cell proliferation and memory enhancement

Seokhwi Kim[1], Nury Kim[2], Jinsu Lee[3], Sungsoo Kim[3], Jongryul Hong[3], Seungkyu Son[3], Won Do Heo[2,3,4]*

Activation of Fas (CD95) is observed in various neurological disorders and can lead to both apoptosis and prosurvival outputs, yet how Fas signaling operates dynamically in the hippocampus is poorly understood. The optogenetic dissection of a signaling network can yield molecular-level explanations for cellular responses or fates, including the signaling dysfunctions seen in numerous diseases. Here, we developed an optogenetically activatable Fas that works in a physiologically plausible manner. Fas activation in immature neurons of the dentate gyrus triggered mammalian target of rapamycin (mTOR) activation and subsequent brain-derived neurotrophic factor secretion. Phosphorylation of extracellular signal–regulated kinase (Erk) in neural stem cells was induced under prolonged Fas activation. Repetitive activation of this signaling network yielded proliferation of neural stem cells and a transient increase in spatial working memory in mice. Our results demonstrate a novel Fas signaling network in the dentate gyrus and illuminate its consequences for adult neurogenesis and memory enhancement.

INTRODUCTION

A cellular signaling network can exhibit complex responses to various external stimuli. Recent advances in optogenetics have enabled researchers to spatiotemporally manipulate signaling pathway components, providing insights into how signaling pathways are dynamically regulated. Each component of the signaling pathway is now considered to react differentially upon the various modes of stimulus (*1*). The optogenetic investigation of a signaling network can demonstrate not only the spatiotemporal modulation of the signaling pathway but also its cellular and organ-level consequences and the signaling dysfunctions seen in numerous diseases (*2*).

Fas receptor (Fas/CD95/APO-1) signaling is an example of a complex network with various downstream outputs. The Fas receptor belongs to the tumor necrosis factor receptor superfamily, whose members play a well-known role as death receptors responsible for initiating the extrinsic apoptotic pathway (*3*). In addition to inducing apoptosis, Fas activation can also induce prosurvival signaling components, such as c-Jun N-terminal kinase (JNK), nuclear factor κB, and AKT-mTOR (mammalian target of rapamycin), depending on the cell type and circumstances (*4*, *5*). Fas-induced nonapoptotic signaling is frequently encountered in the diseased brain, and Fas overexpression is seen in various neurological disorders, such as inflammatory diseases, neurodegenerative diseases, and cerebral ischemia (*5*, *6*). However, controversies exist regarding the mode of activation of Fas downstream components in these circumstances. The involvement of hippocampal Fas activation on cognitive function and memory has long been debated, as both cognitive improvement and impairment have been observed in experiments performed using Fas-deficient (*4*, *7*) or Fas-knockout (*8*) mice. Considering that Fas is overexpressed in the diseased brain and the Fas signaling network is highly complex, we hypothesized that an investigation of dynamic Fas signaling using an inducible activation system could potentially provide a comprehensive explanation for the controversial findings that exist in the literature.

[1]Graduate School of Medical Science and Engineering, Korea Advanced Institute of Science and Technology (KAIST), Daejeon, Republic of Korea. [2]Center for Cognition and Sociality, Institute for Basic Science (IBS), Daejeon, Republic of Korea. [3]Department of Biological Sciences, KAIST, Daejeon, Republic of Korea. [4]KAIST Institute for the BioCentury, KAIST, Daejeon, Republic of Korea.
*Corresponding author. Email: wondo@kaist.ac.kr

RESULTS

Development of the optogenetically activatable Fas receptor

We developed an optogenetically activatable Fas module (optoFAS) consisting of a membrane-anchoring sequence (Lyn), the cytoplasmic domain of Fas (cyFAS), the PHR domain of cryptochrome 2 (CRY2PHR), and enhanced green fluorescent protein (EGFP) (Fig. 1A). Using the ability of CRY2PHR to homo-oligomerize in response to blue light (wavelength, 488 nm), we were able to activate the cloned receptor as previously described (*9*–*11*). When transfected into HeLa cells, optoFAS could successfully induce apoptosis in response to light (Fig. 1B). Transfection of a module lacking CRY2PHR (Lyn-cyFAS-EGFP) could not lead to the apoptosis, implying that the activation of optoFAS is dependent on the oligomerization property of CRY2PHR. We also identified that optoFAS worked with high sensitivity and specificity (fig. S1, A to F). The induced apoptotic level of the cells was superior to that obtained with a previously described chemically inducible system (*12*) or treatment with soluble Fas ligand (100 ng/ml) or cisplatin (10 μg/ml; Fig. 1C). Moreover, upon illumination, we were able to visualize the activation of downstream caspases (Fig. 1, D to G) by real-time imaging using fluorescent protein exchange biosensors (*13*).

Neurons and astrocytes are known to resist to undergo apoptosis by expressing inhibitory molecules to the various steps of the Fas-induced apoptotic pathway (*6*). One such molecule is cellular FLICE (FADD-like IL-1β-converting enzyme)–inhibitory protein (c-FLIP), whose function is a decoy molecule for the activated Fas receptor complex to block the subsequent caspase activation (*14*). We identified that DIV (days in vitro) 7 neurons and astrocytes did not undergo apoptosis upon Fas activation and showed higher levels of c-FLIP expression, as expected (fig. S1, G, H, I, and K). Instead, light stimulation could induce the activation of nonapoptotic signaling components in optoFAS-transfected cultured hippocampal neurons. Using the JNK-KTR (kinase translocation reporter) sensor (*15*), we observed JNK activation in optoFAS-transfected DIV 7 neurons upon illumination (Fig. 1H). Activation of the AKT-mTOR pathway could be identified by immunocytochemical (ICC) staining of pS6 (Fig. 1, I and J). On the other hand, oligodendrocytes that are susceptible to the apoptosis upon Fas activation with low levels of c-FLIP expression revealed decreased cell survival upon optoFas activation (fig. S1, J and K). Together, these results show that

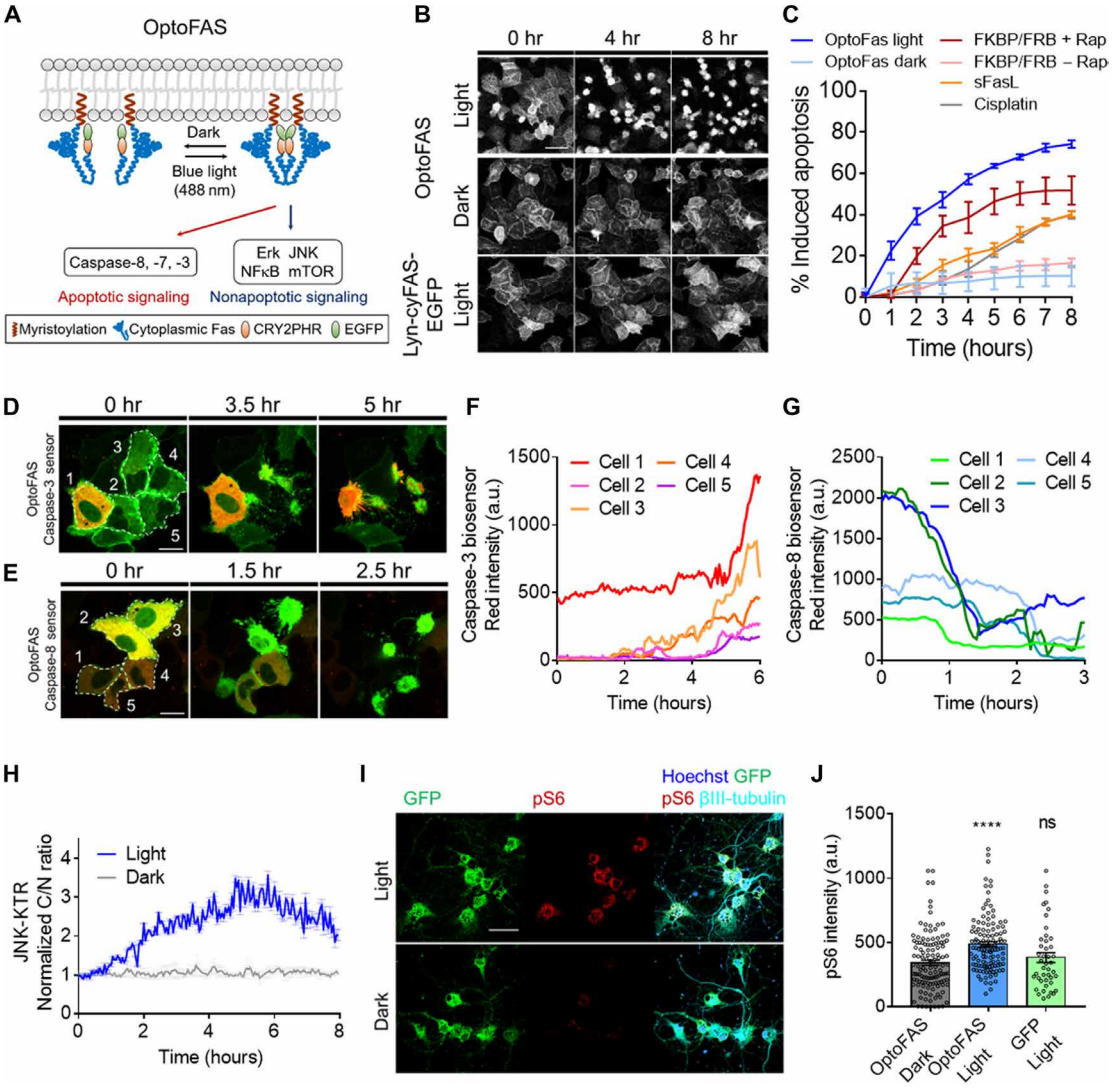

Fig. 1. Development and validation of the optogenetically activatable Fas receptor. (**A**) Schematic diagram of optoFAS and downstream signaling pathways. NFκB, nuclear factor κB. (**B**) Representative confocal images of apoptosis induced in optoFAS-transfected HeLa cells exposed to light stimulation, as compared to optoFAS-transfected cells incubated in the dark and Lyn-cyFAS-EGFP–transfected cells subjected to light stimulation. Scale bar, 50 μm. (**C**) Quantification of the apoptotic induction of HeLa cells over time. OptoFAS light, cells expressing optoFAS subjected to continuous blue light of 5 μW/mm^2; OptoFAS dark, the same cells incubated in dark; FKBP/FRB + Rap, cells transfected with Lyn-cyFAS-FKBP-EGFP and Lyn-cyFAS-FRB-mCherry treated with 500 nM rapamycin; FKBP/FRB − Rap, the same cells without rapamycin treatment; sFasL, treatment with soluble Fas ligand (100 ng/ml); cisplatin, treatment with cisplatin (10 μg/ml; $n \geq 80$ cells per group). (**D**) Representative confocal images of optoFAS- and caspase-3 biosensor–transfected HeLa cells undergoing apoptosis, showing the activation of caspase-3. Scale bar, 20 μm. (**E**) Representative confocal images of optoFAS- and caspase-8 biosensor–transfected HeLa cells undergoing apoptosis, showing the activation of caspase-8. Scale bar, 20 μm. (**F**) Quantification of caspase-3 biosensor activity for the cells shown in (D). (**G**) Quantification of caspase-8 biosensor activity for the cells shown in (E). a.u., arbitrary units. (**H**) Activation of JNK in optoFAS-transfected cultured hippocampal neurons at DIV (days in vitro) 7 with and without illumination, as revealed by the JNK-KTR sensor ($n = 20$ cells were included in the both light and dark groups). (**I**) Representative immunocytochemical (ICC) staining images of optoFAS-transfected cells with or without light stimulation, showing pS6 expression. Scale bar, 50 μm. (**J**) Quantification of the data shown in (I). Data are given as means ± SEM; $n \geq 100$ cells per each group. Two-way analysis of variance (ANOVA) was used for statistical analysis. ****$P < 0.0001$. ns, not significant.

our newly developed optoFAS could induce both apoptotic and nonapoptotic signaling in the proper cell types and thus reflected a physiologically plausible mode of action.

Dynamic Fas signaling network in the dentate gyrus revealed by optogenetic activation

To investigate the dynamics of Fas signaling in the brain in the context of cognition and memory, we injected adeno-associated virus vectors (AAVs) into the 8-week-old mouse hippocampal dentate gyrus (DG). By combining Nestin-Cre and hSyn-DIO vectors, we were able to target immature neurons of the DG for expression as previously described (*16*), which was seen approximately 3 weeks after injection (Fig. 2, A and B, and fig. S2, A to C). Light stimulation of the optoFAS-transduced region could be used to induce the different activation modes of the downstream signaling components. pS6, which is a downstream signaling component of Akt-mTOR, was induced immediately upon

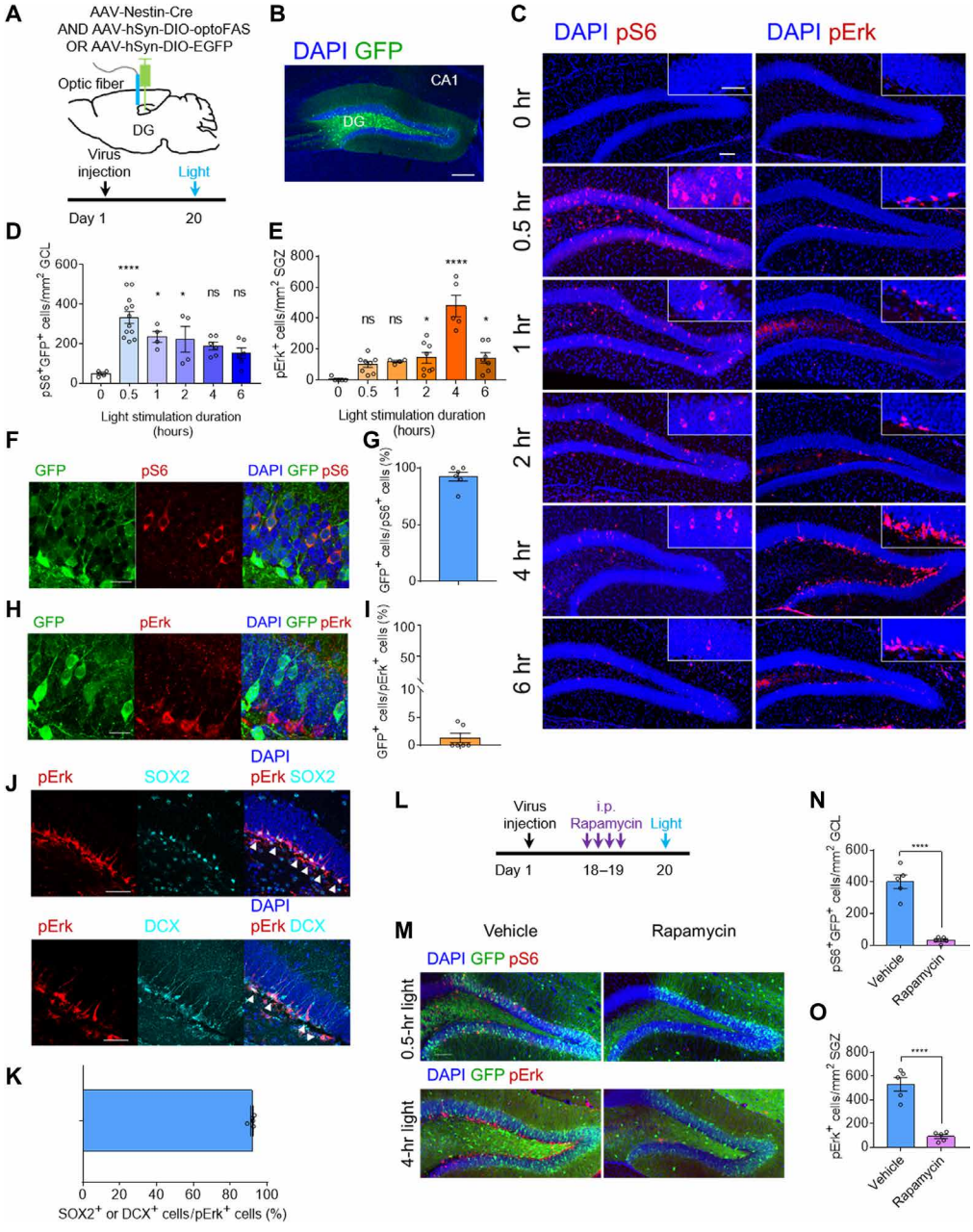

Fig. 2. Optogenetic activation of Fas reveals a dynamic signaling network in the DG. (**A**) A schematic representation and timeline showing the viral injection and experimental procedures. (**B**) A representative image showing the expression of AAV-Nestin-Cre and AAV-hSyn-DIO-optoFAS in the DG. Scale bar, 200 μm. DAPI, 4′,6-diamidino-2-phenylindole. (**C**) Representative images of changes in the levels of pS6 and pErk in the optoFAS-transduced DG as the duration of illumination increased. Inset shows a representative focus area. Scale bars, 100 μm and 50 μm (inset). (**D**) Quantification of the $pS6^+$ cells in (C). Data are presented as means ± SEM; $n \geq 4$ mice were included under each condition. One-way ANOVA was used for statistical analysis. $^{****}P < 0.0001$ and $^{*}P < 0.05$. (**E**) Quantification of the $pErk^+$ cells in (C). Data are presented as means ± SEM; $n \geq 4$ mice were included under each condition. One-way ANOVA was used for statistical analysis. $^{****}P < 0.0001$ and $^{*}P < 0.05$. (**F**) Representative images showing the colocalization of GFP^+ cells and $pS6^+$ cells. Scale bar, 20 μm. (**G**) Quantification of (F). Data are presented as means ± SEM; $n = 6$ mice. A single section per mouse was randomly selected. $n \geq 20$ $pS6^+$ cells were included in each section. (**H**) Representative images showing the lack of colocalization of GFP^+ cells and $pErk^+$ cells. Scale bar, 20 μm. (**I**) Quantification of data shown in (H). Data are presented as means ± SEM; $n = 6$ mice. A single section per mouse was randomly selected. $n \geq 20$ $pErk^+$ cells were included in each section. (**J**) $pErk^+$ cells in the SGZ counterstained with the neural stem cell markers, SOX2 (top) and DCX (bottom). Arrowheads indicate cells with colocalizing signals. Scale bars, 50 μm. (**K**) The proportion of either $SOX2^+$ or DCX^+ cells among all $pErk^+$ cells. Data are presented as means ± SEM; $n = 5$ mice. A single section per mouse was randomly selected. $n \geq 20$ $pErk^+$ cells were included in each section. (**L**) A schematic diagram and timeline showing the rapamycin-induced blockade of the mTOR pathway in vivo. i.p., intraperitoneal. (**M**) Representative images of the effect of mTOR blockage on pS6 and the pErk level. Scale bar, 100 μm. (**N**) Quantification of the $pS6^+$ cells in (M, top row). Data are presented as means ± SEM; $n = 5$ mice per group, four sections per mouse were randomly selected. An unpaired two-tailed *t* test was used for statistical analysis. $^{****}P < 0.0001$. (**O**) Quantification of the $pErk^+$ cells in (M, bottom row). Data are presented as means ± SEM; $n = 5$ mice per group, four sections per mouse were randomly selected. An unpaired two-tailed *t* test was used for statistical analysis. $^{****}P < 0.0001$.

illumination, most notably at 0.5 hours (Fig. 2, C and D), whereas phosphorylation of extracellular signal–regulated kinase (pErk) was activated later, with maximal levels seen after 4 hours of illumination (Fig. 2, C and E). Considering that pS6$^+$ cells were identified by immunohistochemical (IHC) staining of pS6 S240/S244 and pS6 S235/236, we could suggest the specific induction of mTORC1 by optoFAS activation (fig. S3, A and B). pS6$^+$ cells expressed GFP, implying that they were optoFAS-transduced immature neurons (Fig. 2, F and G). However, the pErk$^+$ cells observed in the subgranular zone (SGZ) lacked optoFAS (Fig. 2, H and I). IHC staining for sex determining region Y-box 2 (SOX2) and doublecortin (DCX) revealed that the pErk$^+$ cells in the SGZ were at the developmental stages of neural stem or progenitor cells (Fig. 2, J and K). The 0.5-hour light condition following the 3.5-hour dark condition did not induce pErk at a level comparable to that seen following the 4-hour stimulation, implying that a continuous 4-hour stimulation is required to induce the maximal pErk level in the SGZ (fig. S4, A and B). Light stimulation for 0.5 hours followed by keeping the mice in the dark for 3.5 hours yielded a reduced level of pS6, suggesting that the pS6 level diminishes following its maximal activation at 0.5 hours. Light stimulation for 0.25 hours did not elicit pS6 to a level comparable to that seen after a 0.5-hour light stimulation, indicating that at least 0.5 hours of stimulation is required to maximally activate the mTOR pathway (fig. S4, A and C). Twelve-hour dark incubation following the illumination declined the elevated pS6 and pErk level to those of nonstimulated samples. However, when the light stimulation was repeated (4 hours/day for three or five times), the number of pErk$^+$ cells in SGZ was remained to be elevated to a certain level despite the 12-hour dark incubation (fig. S4, D and E), implying that the repetitive stimulation of Fas in immature neurons induces prolongation of ERK activation of neural stem cells. On the other hand, the level of pS6 with the repetitive stimulation and the following dark incubation was similar to that of unstimulated samples (fig. S4, D and F). Intraperitoneal injection of rapamycin, which was intended to block the mTOR pathway in optoFAS-transduced mice, suppressed pS6 in the granular cell layer (GCL) and pErk in the SGZ of the hippocampal DG (Fig. 2, L to O). These results imply that the Fas-mediated activation of the mTOR pathway in immature neurons is related to the subsequent elevation of the pErk level in neural stem cells.

Evidence of mTOR and Erk activation could be identified in human disease samples and mouse models showing Fas overexpression. We conducted gene set enrichment analysis (GSEA) of the hippocampi of patients with Alzheimer's disease (Gene Expression Omnibus: GSE84422) (*17*) using a public database (www.ncbi.nlm.nih.gov/geo). When resorting the patients with Alzheimer's disease into mild [clinical dementia rating (CDR), 0.5 and 1] and severe (CDR, 3 to 5) cases and analyzed the FAS-PATHWAY gene signature (M9503), we identified elevated Fas expression in mild cases of Alzheimer's disease compared to the healthy controls and severe cases (fig. S5, A to C). AKT-MTOR up-regulated gene signature was enriched in mild cases of Alzheimer's disease compared to healthy control or severe cases (fig. S5, D to F). In addition, mitogen-activated protein kinase (MAPK) up-regulated signature was enriched in mild cases of Alzheimer's disease compared to healthy control or severe cases (fig. S5, G to I). Up-regulated gene signature of the AKT-mTOR and MAPK pathway in Fas-overexpressed human hippocampal samples provides additional support on our findings. In addition, activation of pErk in the SGZ was also observed in the brains of mice exposed to intracerebroventricular injection of lipopolysaccharide (LPS) and those of Alzheimer model (5XFAD) mice, both of which showed the high-level Fas expression (fig. S5, J to N).

Brain-derived neurotrophic factor secretion in immature neurons upon Fas activation

In an effort to identify some of the mediating factors that lie between the activation of mTOR in immature neurons and that of Erk in neural stem cells, we examined three candidate molecules that are known to contribute to regulating the neural stem cell population (*18*–*20*). In a cell culture system, DIV 7 hippocampal neurons showed rapid declines of the neural stem cell markers, SOX2 and DCX, but an increase in calretinin, which is expressed in immature neurons undergoing differentiation (fig. S6, A and B). Brain-derived neurotrophic factor (BDNF) mRNA expression gradually increased in optoFAS-transduced DIV 6 neurons following illumination (Fig. 3, A and B). Another candidate, insulin-like growth factor 1 (IGF-1), was robustly increased, while the other, interleukin-6 (IL-6), was decreased (Fig. 3, C and D). To confirm the activation of Fas upon illumination, we analyzed the transcriptional changes of NeuroD (fig. S7, A and B) and Hes5 (fig. S7C) upon light stimulation, which was previously described (*4*). Treatment of the cultured cells with the mTOR pathway inhibitor, rapamycin, suppressed both the pS6 level (fig. S8, A to C) and the mRNA expression of BDNF (Fig. 3, E and F). This is consistent with the previous report that the transcription of BDNF is downstream of mTOR signaling in the Fas network (*21*). The transcriptional increase in IGF-1 by optoFAS activation was not affected by rapamycin treatment (Fig. 3G). The illumination-induced secretion of BDNF by optoFAS-transduced neurons was confirmed by performing BDNF enzyme-linked immunosorbent assay (ELISA) using supernatants from the cultured neuron plates (Fig. 3H). Administration of the BDNF/tropomyosin receptor kinase B (TrkB) inhibitor, ANA-12, to optoFAS-injected mice yielded a significant decrease in the number of pErk$^+$ cells in the SGZ following light stimulation, supporting the hypothesis that BDNF from the immature neurons induces pErk activation in neural stem cells (fig. S8, D to F). Cultured neurons of neural stem cells or neural progenitor cell stages (DIV 1 to DIV 2) were responsive to the exogenous BDNF treatment (200 ng/ml) to induce ERK activation (*15*) regardless of their preincubation with rapamycin (fig. S9, A and B). Treatment of the concentrated supernatant from light-stimulated immature neurons (DIV 7) induced ERK activation in DIV 1 to DIV 2 neurons. Given that the ERK activation has not resulted from the supernatants of ANA-12–pretreated DIV 7 neurons, it is plausible to conclude that BDNF included in the stimulated supernatant leads to the observed ERK level change (fig. S9, C and D). In addition, the supernatant from rapamycin-pretreated DIV 7 neurons had failed to induce ERK activation, although the recipient DIV 1 neurons were still responsive to exogenous BDNF (fig. S9, E and F), implying that ERK activation in neural stem cells is resulted from the mTOR-induced BDNF secretion by Fas activation in immature neurons. To further investigate whether the secretion of BDNF from the immature neurons elicits Erk activation in neural stem cells in vivo, we injected AAV-Nestin-Cre and AAV-hSyn-DIO-optoFAS into the DG of BDNF-floxed mice ($Bdnf^{flox/flox}$; Fig. 3I). While the number of pS6$^+$ cells in the GCL was not significantly altered (Fig. 3, J and K), $Bdnf^{flox/flox}$ mice exhibited significantly fewer pErk$^+$ cells in the SGZ upon illumination (Fig. 3, J and L) compared to their littermates. From these observations, we concluded that there is a paracrine signaling network in the DG whereby prolonged Fas activation in

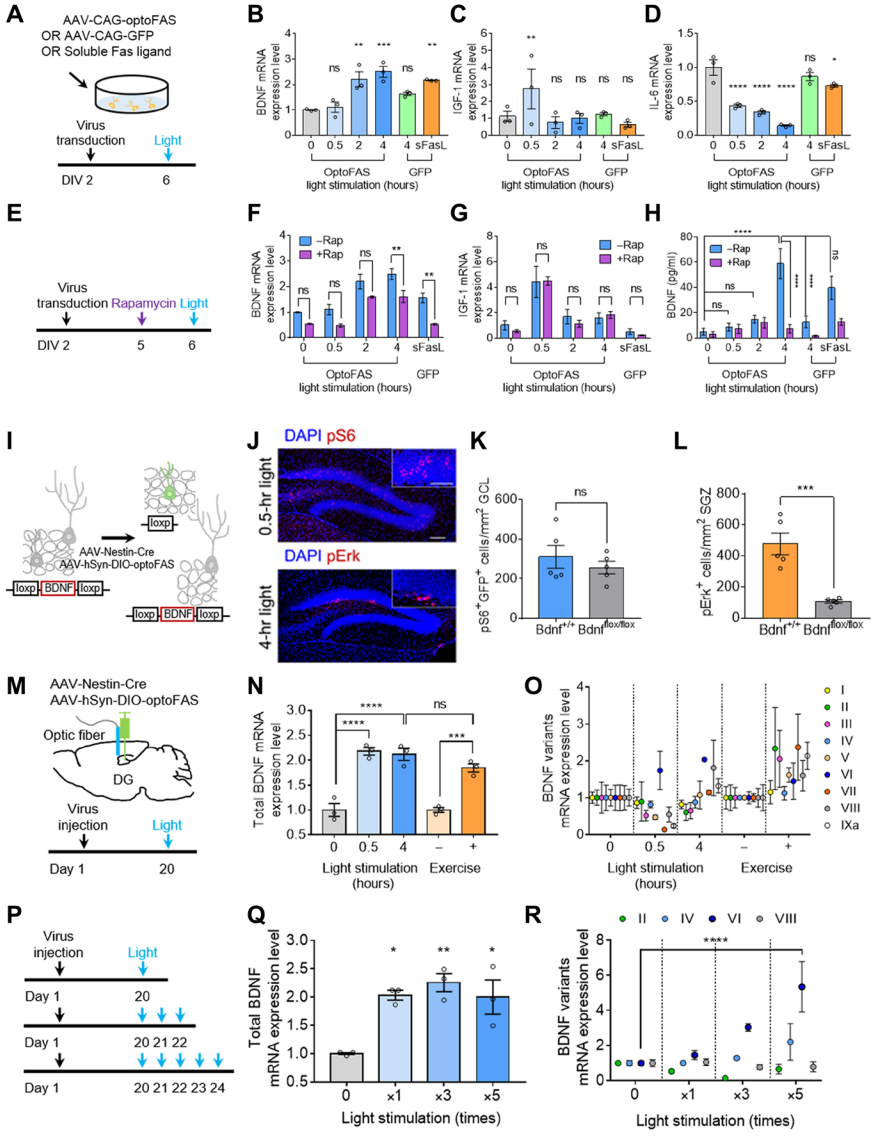

Fig. 3. Optogenetic stimulation of Fas in immature neurons induces BDNF secretion, working as a paracrine mediator. (**A**) A schematic diagram and timeline for the viral transduction and light stimulation of cultured hippocampal neurons. (**B** to **D**) Quantitative real-time polymerase chain reaction (qRT-PCR) results for BDNF (B), IGF-1 (C), and IL-6 (D) in optoFAS-transduced neurons exposed to light stimulation, GFP-transduced neurons exposed to light stimulation, and GFP-transduced neurons treated with soluble Fas ligand. Data are presented as means ± SEM; $n = 3$ per group. One-way ANOVA was used for statistical analysis. $^{**}P < 0.01$, $^{***}P < 0.001$, and $^{****}P < 0.0001$. (**E**) A schematic illustration and timeline for the viral transduction, rapamycin treatment, and light stimulation of cultured hippocampal neurons. (**F** and **G**) qRT-PCR results for BDNF (F) and IGF-1 (G) in optoFAS-transduced neurons treated with rapamycin and exposed to light stimulation and GFP-transduced neurons treated with soluble Fas ligand. Data are presented as means ± SEM; $n = 3$ per group. Two-way ANOVA was used for statistical analysis.$^{**}P < 0.01$. (**H**) The results of BDNF ELISA for the supernatants of optoFAS-transduced neurons exposed to light stimulation, GFP-transduced neurons exposed to light stimulation, and GFP-transduced neurons treated with Fas ligand. Data are presented as means ± SEM; $n \geq 3$ per group. Two-way ANOVA was used for statistical analysis. $^{****}P < 0.0001$. (**I**) A schematic illustration showing how immature neurons in the *Bdnf*$^{flox/flox}$ mouse are targeted to acquire deficits in BDNF transcription via transduction of AAV-Nestin-Cre and AAV-hSyn-DIO-optoFAS. (**J**) Representative images of pS6 (top) and pErk (bottom) IHC staining of a *Bdnf*$^{flox/flox}$ mouse transduced by AAV-Nestin-Cre and AAV-hSyn-DIO-optoFAS and subjected to illumination. Inset shows a representative focus area. Scale bars, 100 μm and 50 μm (inset). (**K**) Quantification of the pS6$^+$ cells in (J) and comparison to that of *Bdnf*$^{+/+}$ mice. Data are presented as means ± SEM; $n = 5$ mice. Four sections per mouse were randomly selected. An unpaired two-tailed *t* test was used for statistical analysis. (**L**) Quantification of the pErk$^+$ cells in (J) and comparison to that in *Bdnf*$^{+/+}$ mice. Data are presented as means ± SEM; $n = 5$ mice. Four sections per mouse were randomly selected. An unpaired two-tailed *t* test was used for statistical analysis. $^{***}P < 0.001$. (**M**) A schematic diagram and timeline for viral injection and experimental procedure for qRT-PCR of mouse hippocampal tissue. (**N**) Total BDNF mRNA expression level in brains from optoFAS-transduced mice exposed to light stimulation and from exercised mice. Data are presented as means ± SEM; $n = 3$ per group. One-way ANOVA was used for statistical analysis. $^{****}P < 0.000$ and $^{***}P < 0.001$. (**O**) mRNA expression levels for the splicing variants of BDNF in the optoFAS-transduced mouse brain and exercised mouse brain. Data are expressed as means ± SEM; $n = 3$ per group. (**P**) Timeline for viral injection and experimental procedure for qRT-PCR of mouse hippocampal tissue following exposure to repetitive stimulation. (**Q**) Total BDNF mRNA expression level in optoFAS-transduced hippocampus subjected to single or repetitive light stimulation. Data are presented as means ± SEM; $n = 3$ per group. One-way ANOVA was used for statistical analysis. $^{*}P < 0.05$ and $^{**}P < 0.01$. (**R**) The mRNA expression levels of BDNF II, IV, VI, and VIII in optoFAS-transduced hippocampus subjected to single or repetitive light stimulation. Data are presented as means ± SEM; $n = 3$ per group. One-way ANOVA was used for statistical analysis. $^{****}P < 0.0001$.

immature neurons induces the release of BDNF, which then activates ERK in neural stem cells.

Transcription of BDNF VI upon optogenetic activation of Fas in immature neurons

We next questioned how BDNF secreted from immature neurons could induce pErk activation specifically in neural stem cells. Quantitative real-time polymerase chain reaction (qRT-PCR) revealed that the transcription of total BDNF was elevated in optoFAS-transduced hippocampal tissue upon light stimulation, to a level similar to that seen in an exercised hippocampus (Fig. 3, M and N). However, unlike exercise, optoFAS activation preferentially increased the transcription of BDNF VI among the BDNF splicing variants (Fig. 3O). Repetitive stimulation (4 hours per each round) of optoFAS in the DG markedly increased the BDNF VI transcription level without notably altering that of total BDNF, regardless of the number of stimulation rounds (Fig. 3, P to R). Considering that BDNF splicing variants exhibit distinct subcellular localizations and play spatially restricted roles (*22*), BDNF VI may code spatial information and direct ERK activation only in the SGZ.

Adult hippocampal neurogenesis induced by repetitive activation of Fas

Since ERK signaling plays a crucial role in cellular proliferation, we investigated whether the proliferation of neural stem cells could be induced via the Fas signaling network we found. OptoFAS- or GFP-transfected 10-week-old mice were intraperitoneally injected with 5-bromo-2′-deoxyuridine (BrdU) and exposed to light stimulation (Fig. 4A). Repetitive light stimulation (4 hours per each round) of the optoFAS-transduced DG induced the proliferation of neural stem cells, which was identified by an increase in $BrdU^+$ cells (Fig. 4B). IHC staining of SOX2 and DCX confirmed that the cells were neural stem or progenitor cells (Fig. 4, C and D). After a 1-week incubation, the optoFAS-stimulated mice showed a statistically significant increase in BrdU and calretinin double-positive cells in the DG, implying that the proliferated stem cells had undergone differentiation, leading to adult neurogenesis (Fig. 4, E to G). Administration of rapamycin to block the mTOR pathway significantly decreased the number of $BrdU^+$ cells upon light stimulation, confirming that this adult neurogenesis was induced by the novel Fas signaling network revealed herein (Fig. 4, H to J).

Spatial memory increase by repetitive activation of Fas signaling network

We next investigated whether this Fas signaling network could affect behavior related to hippocampus-dependent memory. Since the DG has been well recognized for its involvement in spatial working memory (*23*), we subjected optoFAS- or GFP-transduced mice to the Y-maze test and monitored the change in spontaneous alteration behavior upon light stimulation. A single round of light stimulation for 4 hours did not alter the spontaneous alteration in optoFAS-injected mice, as tested 1 day after the stimulation; however, repetition (five rounds) of stimulation significantly increased the percentage of spontaneous alteration at this time point (Fig. 5, A and B). This elevation of spontaneous alteration in repetitively stimulated optoFAS-transduced mice was not observed in samples obtained at days 7, 14, and 28 after stimulation, implying that the phenomenon is transient (Fig. 5, D and E). To confirm that this behavioral alteration was mediated via our novel Fas signaling network, we used rapamycin (Fig. 5G) or ANA-12 (Fig. 5J) to block the mTOR pathway or BDNF/TrkB signaling, respectively. Both treatments suppressed the elevation of spontaneous alteration in optoFAS-activated mice (Fig. 5, H and K). The total entries into the Y-maze arms did not significantly differ across the experimental groups (Fig. 5, C, F, I, and L) nor did the locomotor function or anxiety level revealed by open-field tests of the mice differ among the groups in any experiment (fig. S10, A to X). Thus, our findings reveal that repetitive activation of the identified Fas signaling network induces a transient increase in spatial working memory in mice.

DISCUSSION

Optogenetic dissection of neural circuits has been used for years to rigorously investigate the regional circuits of the brain related to neurological disorders (*24*). In addition, strategies of controlling the localization of intracellular proteins by light have demonstrated the spatial dissection of the dynamics of endogenous proteins (*25*, *26*). Optogenetic activation of the signaling pathway reveals that each component of the signaling pathway, as well as transcriptome profiles, responds differentially to the various modes of stimulus (*1*, *27*). These examples of applications imply that optogenetics not only can recapitulate the activation of the signaling pathway by its ligand but also can uncover the circumstances that are unable to be investigated by the chemical treatment or traditional transgenic model.

Despite the well-known inducible expression of Fas in brain disorders, we do not yet understand how Fas signaling operates or affects the phenotype. Here, we investigated Fas signaling in the brain using optogenetically activatable Fas, which enabled us to spatiotemporally control the signaling network. We found a novel Fas signaling network in the DG regarding communication between immature neurons and neural stem cells. Transient activation of Fas in immature neurons activates only the mTOR pathway, whereas prolonged activation induces both the mTOR pathway in Fas-expressing immature neurons and the ERK pathway (via secreted BDNF) in neural stem cells lacking Fas expression (Fig. 6A). Moreover, the repetitive activation of this Fas signaling network could result in the proliferation of neural stem cells and a transient increase in spatial working memory (Fig. 6B). To our knowledge, this is the first study that used optogenetic dissection to demonstrate the temporal dynamics of signaling in the DG.

The spatiotemporal coordination of multiple phases of signaling is not uncommon (*28*). In the middle cerebral artery occlusion model, ERK- and AKT-mTOR signaling pathways are observed in distinct populations of neurons, suggesting the independent roles as emergency or maintenance signals for cell survival (*29*). Considering that Fas is overexpressed in the ischemic brain, the aforementioned findings might be related to the Fas signaling network as well. Another possible evidence of the Fas signaling network we described is activation of ERK in neural stem cells of the DG in a mouse epilepsy model (*30*), an example of Fas-overexpressed disease condition (*31*). An interesting finding in this study was that a BDNF splicing variant, BDNF VI, was selectively expressed upon the repetitive activation of Fas in immature neurons of DG. The "addiction" of BDNF splicing variants has been observed in the dendritic development of neurons (*22*) and in the hippocampus throughout the life span (*32*). The utilization of in vivo visualizing techniques such as BDNF-Live-Exon-Visualization (*33*) will enable further investigation regarding how different BDNF splicing variants dynamically play roles in these circumstances.

A pivoting role of Fas in the survival of neural stem cells and their lineage commitment has been widely accepted (*4*, *34*, *35*). However,

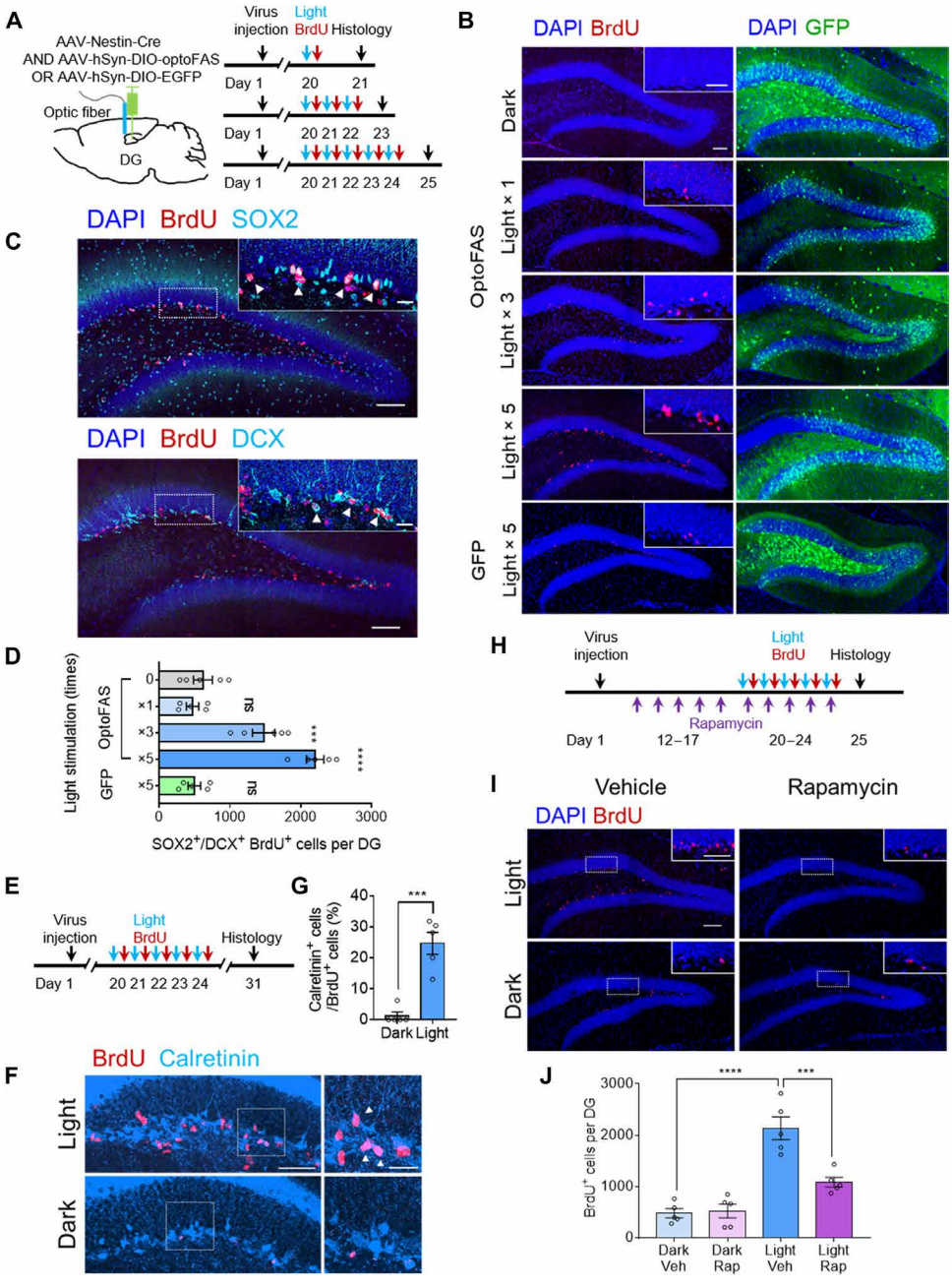

Fig. 4. Repetitive activation of Fas induces adult hippocampal neurogenesis. (**A**) A schematic illustration and timeline of the experiment used to evaluate neural stem cell proliferation following a single or repetitive light stimulation of the optoFAS-transduced mouse brain. (**B**) Representative images of neural stem cell proliferation upon light stimulation, as assessed by BrdU IHC staining (left column; inset, a representative focus area) and images of optoFAS expression in each case (right column). Scale bars, 100 μm and 50 μm (inset). (**C**) $BrdU^+$ cells in the SGZ following five rounds of light stimulation, in sections counterstained for SOX2 and DCX (inset shows the boxed region; arrowheads represent cells with colocalizing signals). Scale bars, 100 μm and 20 μm (inset). (**D**) Quantification of the $BrdU^+SOX2^+$ or $BrdU^+DCX^+$ cells in the DG following single or repetitive light stimulation of optoFAS-transduced mouse brain. Data are presented as means ± SEM; $n = 5$ mice under each condition. One-way ANOVA was used for statistical analysis. $^{***}P < 0.001$ and $^{****}P < 0.0001$. (**E**) Timeline of the experiment for evaluating adult neurogenesis upon repetitive optoFAS stimulation. (**F**) Representative images of $BrdU^+$ cells counterstained for calretinin. Right: An enlargement of the boxed region in the left image; arrowheads indicate cells with colocalizing signals. Scale bars, 50 μm (left) and 20 μm (right). (**G**) Quantification of the data shown in (F). Data are presented as means ± SEM; $n = 5$ mice under each condition. An unpaired two-tailed t test was used for statistical analysis. $^{***}P < 0.001$. (**H**) Timeline of the experiment used to evaluate neural stem cell proliferation upon blockage of the mTOR pathway in optoFAS-transduced mouse brain. (**I**) Representative images of $BrdU^+$ cells in optoFAS-transduced DG subjected to rapamycin treatment (inset shows the boxed region). Scale bars, 100 μm and 50 μm (inset). (**J**) Quantification of the data shown in (I). Data are presented as means ± SEM; $n = 5$ mice under each condition. One-way ANOVA was used for statistical analysis. $^{****}P < 0.0001$ and $^{***}P < 0.001$.

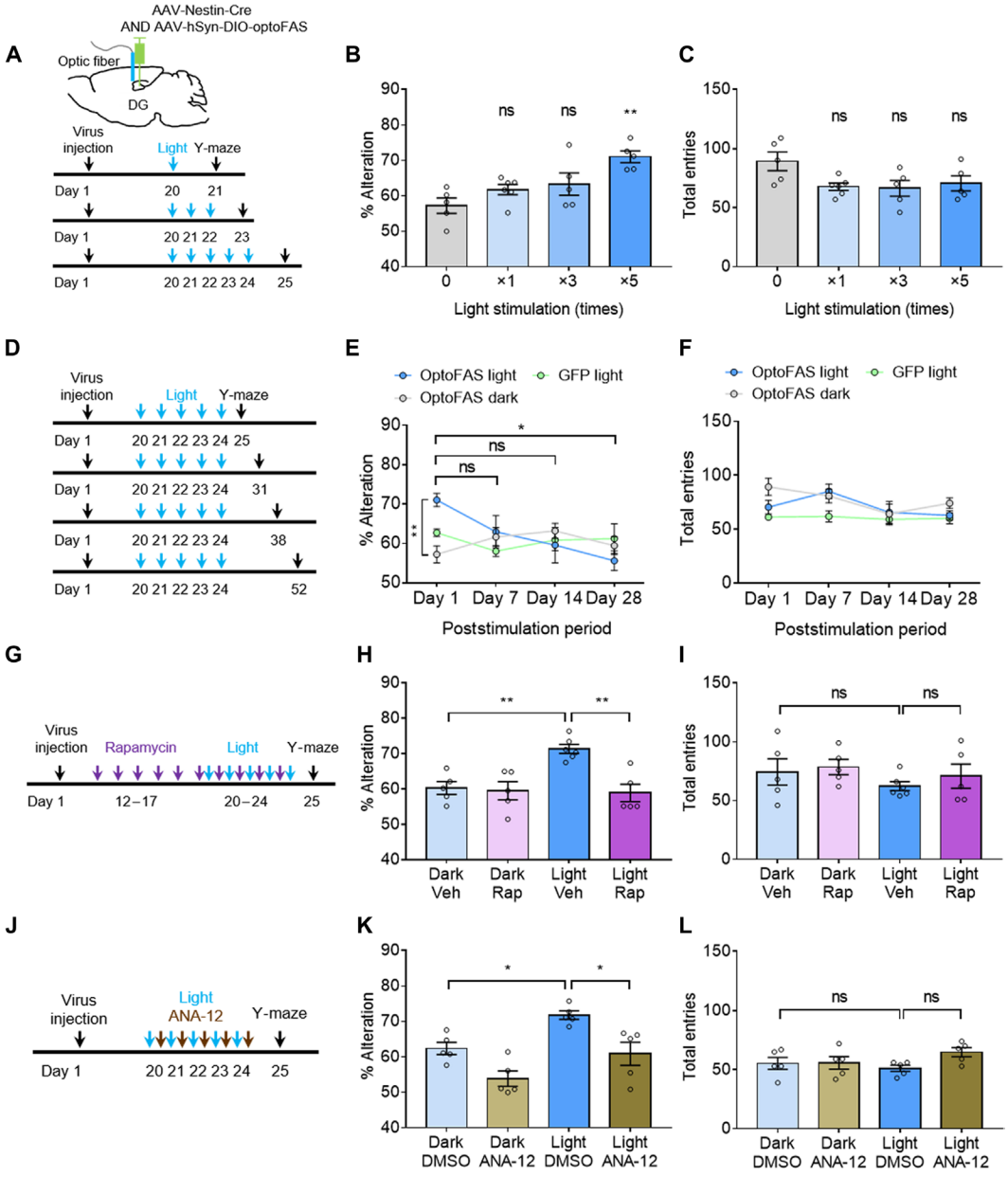

Fig. 5. Repetitive activation of the Fas signaling network induces transient memory increase. (**A**) A schematic illustration and timeline for the behavioral tests used to assess optoFAS-transduced mice with light stimulation. (**B**) Spontaneous alteration on Y-maze tests of the optoFAS-transduced mice exposed to single or repetitive light stimulation. Data are presented as means ± SEM; $n = 5$ to 6 mice per group. One-way ANOVA was used for statistical analysis. $^{**}P < 0.01$. (**C**) Total entries on Y-maze tests among optoFAS-transduced mice exposed to a single or repetitive light stimulation. Data are presented as means ± SEM; $n = 5$ to 6 mice per group. One-way ANOVA was used for statistical analysis. (**D**) Timeline for the behavioral tests of optoFAS- or GFP-transduced mice given prolonged incubation after light stimulation. (**E**) Spontaneous alteration on Y-maze tests among optoFAS- or GFP-transduced mice subjected to five rounds of light stimulation followed by varying durations of incubation. Data are presented as means ± SEM; $n = 5$ mice per group. One-way ANOVA was used for statistical analysis. $^{*}P < 0.05$. (**F**) Total entries on Y-maze tests among optoFAS- or GFP-transduced mice subjected to five rounds of light stimulation, followed by varying durations of incubation. Data are presented as means ± SEM; $n = 5$ mice per group. One-way ANOVA was used for statistical analysis. (**G**) Timeline for the behavioral tests of optoFAS-transduced mice exposed to light stimulation in the presence of mTOR pathway blockade. (**H**) Spontaneous alteration on Y-maze tests among optoFAS-transduced mice subjected to repetitive stimulation and rapamycin treatment. Data are presented as means ± SEM; $n = 5$ to 6 mice per group. One-way ANOVA was used for statistical analysis. $^{**}P < 0.01$. (**I**) Total entries on Y-maze tests among optoFAS-transduced mice subjected to repetitive stimulation and rapamycin treatment. Data are presented as means ± SEM; $n = 5$ to 6 mice per group. One-way ANOVA was used for statistical analysis. (**J**) Timeline for the behavioral tests of optoFAS-transduced mice exposed to light stimulation in the presence of BDNF/TrkB blockade. (**K**) Spontaneous alteration on Y-maze tests among optoFAS-transduced mice subjected to repetitive stimulation and ANA-12 treatment. Data are presented as means ± SEM; $n = 5$ mice per group. One-way ANOVA was used for statistical analysis. $^{*}P < 0.05$. DMSO, dimethyl sulfoxide. (**L**) Total entries on Y-maze tests among optoFAS-transduced mice subjected to repetitive stimulation and ANA-12 treatment. Data are presented as means ± SEM; $n = 5$ mice per group. One-way ANOVA was used for statistical analysis.

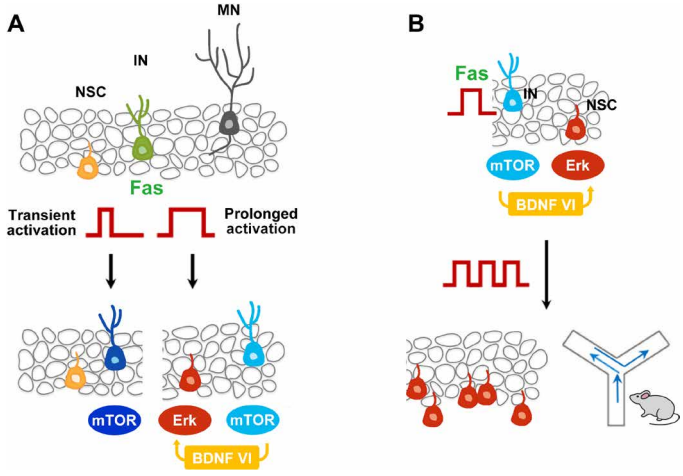

Fig. 6. Summary of molecular and cellular dynamics of Fas signaling in the adult hippocampal DG upon prolonged and repetitive activation. (**A**) Summary of the molecular dynamics of Fas signaling in the DG upon optogenetic Fas activation. Transient Fas activation in immature neurons of the DG induces activation of the mTOR pathway in these cells. Prolonged activation results increases pErk in neural stem cells through BDNF secreted from Fas-activated immature neurons. NSC, neural stem cell; IN, immature neuron; MN, mature neuron. (**B**) Summary of the histological and behavioral outcomes observed following repetitive activation of Fas signaling in the DG. Repetitive activation of the Fas–mTOR (immature neuron)–BDNF VI–pErk (neural stem cell) paracrine pathway in the DG induces the proliferation of neural stem cells and transiently increases spatial working memory.

all the studies had been performed using the Fas-deficient *lpr* mouse model (*36*). Since Fas is overexpressed rather than deficient in the majority of brain illnesses, our work reflects the actual mode of action of Fas. In addition to the discovery of the Fas signaling network leading to the adult neurogenesis herein, we identified that repetitive activation rather than a single bout of the signaling network is required for the neurogenesis. This implies that the proliferation of neural stem cells is the consequence of the repeated alarming signal in the diseased brain by Fas. Given that neural stem cells contribute to cognitive improvement via BDNF in Alzheimer's brain (*37*) and BDNF is preferentially elevated in mice that show increased spontaneous alteration, we speculate that BDNF VI may direct the improvement of spatial working memory in the Fas-activated, compromised brain. The level of adult neurogenesis is well known to be increased in acute neurological disorders, such as stroke (*38*). In chronic diseases, there is some debate regarding changes of adult neurogenesis (*39*, *40*). We propose that the Fas signaling network found in the present work could be responsible for the observed increase in adult neurogenesis in these diseases. Supporting evidence for this idea is that AKT-mTOR and MAPK up-regulated signatures were only observed in patients with mild Alzheimer's disease with increased Fas expression. Alongside, problems with cognition and memory are seldom identified early during the course of a chronic neurological disorder. In patients with Alzheimer's disease, a clinical stage of mild cognitive impairment (i.e., a mildly affected memory level) is commonly seen early in the disease course (*41*). Similar findings have also been reported for other chronic neurological diseases (*42*). Considering that the repetitive activation of optoFAS resulted in a transient memory increase, it is likely that repeated activation of Fas during the early course of a disease can help protect cognitive function and memory to some degree.

In summary, this study found a novel mechanism that links Fas activation in immature neurons to ERK activation in neural stem cells using optogenetically activatable Fas receptor. Spatiotemporal and repetitive activation that is only implemented by optogenetics had enabled us to identify how this signaling network leads to adult neurogenesis. The way that proliferated neural stem cells contribute to the memory after fully matured and integrated into the existing neuronal network in DG remains to be investigated. Instead, the proposed Fas signaling network identified the transient increase in spatial working memory via BDNF as a behavioral consequence of the network. Overall, the present study has implications for the utilization of optogenetics to find the sophisticated role of an in vivo signaling network that has critical importance in understanding the pathophysiology of neurological disorders.

MATERIALS AND METHODS

Plasmids

To construct optoFas, a myristoylation sequence (Lyn) and the CRY2PHR were amplified by PCR from the optically controlled fibroblast growth factor receptor 1 (optoFGFR1) (*10*) and inserted into pEGFP-N1 (Clontech) using NheI/XhoI and BamHI/AgeI digestion. The cyFAS was PCR-amplified from HeLa cell complementary DNA (cDNA) and inserted into the Lyn-PHR-EGFP construct using XhoI/EcoRI digestion. The following primers used were as follows: Lyn, 5′-GTAGCTAGCCACC ATGGGATGTATAAAATCAAAAGG-3′ (forward) and 5′-GTACTCGAGCGCACTACCAGCACTACCAG-3′ (reverse); PHR, 5′-GTAGGATCCCATGAAGATGGACAAAAAGACCA-3′ (forward) and 5′-GTAACCGGTGCGTACACGGCAGCACCGATC-3′ (reverse); Fas, 5′-GTACTCGAGAAGAGAAAGGAAGTACAGAAAACATGCAGA-3′ (forward) and 5′-GTAGAATTCTGACCAAGCTTTGGATTTCATTT-3′ (reverse). AAV-MAG-optoFAS was constructed by Gibson Assembly Cloning (New England Biolabs), which was used to replace EGFP with PCR-amplified optoFAS in the pAAV-MAG-EGFP vector (provided by M. Klugmann, University of New South Wales). AAV-Nestin-Cre was generated by PCR amplification of the Nestin promoter from pNestin-EGFP (Addgene #38777) and Cre from pCAG-iCre (Addgene #89573); the products were subjected to MluI/XbaI and EcoRI/AgeI digestion, respectively, and inserted into the pAAV-CaMKIIa-EGFP vector (Addgene #50469). The following primers were used: Nestin, 5′-GTAACGCGTGGAGCAGGAGAAACAGGGCC-3′ (forward) and 5′-GTATCTAGAAAGTCTTGGAGCCACCGC-3′ (reverse); Cre, 5′-ATGCAGAATTCTTAGTCCCCATCCTCGAGCAG-3′ (forward) and 5′-ATGCAACCGGTGCCACCATGCCCAAGAAGAAG-3′ (reverse). AAV-hSyn-DIO-optoFAS was constructed by replacing EGFP in the pAAV-hSyn-DIO-EGFP vector (Addgene #50457) with optoFAS using PCR amplification and NheI/AscI digestion. The following primers were used: 5′-GTAGCTAGCCACCATGGGATGTATAAAATCAAAAGG-3′ (forward) and 5′-GTAGGCGCGCCCGGCCGCTTTACTTGTACAGC-3′ (reverse). AAV-CAG-optoFAS and AAV-CAG-EGFP were constructed by Gibson Assembly Cloning, which was used to replace the XbaI/EcoRV sequence of the AAV-CAG-FLEX-EGFP vector (Addgene #28304) with optoFAS or EGFP from the pEGFP-N1 vector. The following primers were used: optoFAS, 5′-GTGTGACCGGCGGCTCTAGAGCTAGCCACCATGGGATGTATAAAATCAA-3′ (forward) and 5′-AGGTTGATTCCGGAGATATCGCGGCCGCTTTACTT-3′ (reverse); EGFP, 5′-GTGTGACCGGCGGCTCTAGAGCTAGCCACCATGGTGAGCAAGGGCGAGG-3′ (forward) and 5′-AGGTTGATTCCGGAGATATCGCGGCCGCTTTACTT-3′ (reverse). Lenti-Nestin-EGFP was generated

by Gibson Assembly Cloning; the fragment was PCR-amplified from pNestin-EGFP and inserted into pLenti-CamKIIa-optoSTIM1 (*11*) using PacI/EcoRI digestion. The following primers were used: 5′-CAGAGATCCAGTTTGGTTAATTAACTGCAGGTCGACG-GAGC-3′ (forward) and 5′-GATTATCGATAAGCTTGATATC-GAATTCGCGGCCGCTTTACTTG-3′ (reverse).

Cell culture, reagents, and transfection

HeLa and human embryonic kidney (HEK) 293T cells were cultured in Dulbecco's modified Eagle's medium (DMEM; catalog no. 11965092, Gibco) supplemented with 10% fetal bovine serum (FBS; Invitrogen) and maintained at 37°C and 10% CO_2. Cell lines were confirmed to be contamination-free using an e-MycoTM Mycoplasma PCR detection kit (iNtRON). Ninety-six–well plates (catalog no. 89626, Ibidi) were used for cell culture and live-cell imaging.

Embryos of embryonic day 18 pregnant Sprague-Dawley female rats were used to generate primary cultures of neurons, astrocytes, and oligodendrocytes. For neuron culture, embryos were obtained and placed in Hanks' balanced salt solution (HBSS) (catalog no. 14185-052, Gibco)–*N*-2-hydroxyethylpiperazine-*N*-2-ethane sulfonic acid (HEPES) (10 mM; catalog no. 15630-080, Gibco) solution. Each hippocampus was dissected from the embryonal brain and incubated in 0.25% trypsin for 15 min at 37°C. It was then washed sequentially with HBSS containing 10% FBS, HBSS containing 5% FBS, and HBSS. Trituration was performed with a micropipette, and the solution was passed through a 70-μm filter (Falcon). Neurons were plated on poly-L-lysine (0.1 mg/ml; catalog no. P2636, Sigma-Aldrich)–precoated plates containing plating medium. Neurobasal medium (catalog no. 21103-049, Gibco) supplemented with 2% horse serum (HS; catalog no. 16050122, Gibco), 2% GlutaMAX (catalog no. 35050-061, Gibco), and 2% penicillin-streptomycin (catalog no. 15140-122, Gibco) was used for plating medium. The cultured neurons were incubated at 37°C and 5% CO_2. One hour after plating, the plating medium was replaced with maintenance medium [plating medium lacking HS but containing 2% B-27 (catalog no. 17504-044, Gibco)].

Cultures of rat cortical astrocytes were generated by obtaining the cerebral hemisphere of the embryo and placing it in HBSS-HEPES. Processing was performed as described for the neuronal culture, except that DMEM with 10% FBS was used for the wash and medium. At 1 day after plating, the plated astrocytes were physically dissociated from the culture plate by tapping, and the medium was replaced.

Oligodendrocyte culture was conducted as previously described (*43*) with minor modifications. Oligodendroglial cells were isolated on day 10 of initial culture, from cultures that were preshaken at 200 rpm for 45 min at 37°C. During the maintenance period, half of the medium volume was replaced every other day. To induce differentiation into oligodendrocytes, the maintenance medium was replaced with differentiating medium.

For in vitro experiments, soluble Fas ligand (catalog no. 310-03H, PeproTech) was dissolved in culture medium and used to pretreat samples for 6 hours before each experiment at a concentration of 100 ng/ml unless otherwise specified. Rapamycin (catalog no. R-5000, LC Labs) was dissolved in culture medium (final concentration, 500 nM) and used to pretreat samples for 12 hours before experiments. BDNF (catalog no. PHC7074, Invitrogen) was dissolved in solutions for neuronal starvation and treated at a concentration of 200 ng/ml. ANA-12 (catalog no. 4781, Tocris Bioscience) was treated to the cultured neurons at a concentration of 10 μM.

For HeLa cells (except for the coculture experiments) and neurons, transfection was conducted using Lipofectamine LTX (Invitrogen) according to the manufacturer's instructions. For the transfection of astrocytes and coculture experiments involving HeLa cells, electroporation was performed using a microporator (Neon Transfection System, Invitrogen). The optimized condition for electroporation of HeLa cells was two pulses of 980 V for 35 ms.

Live-cell imaging and photoactivation

A Nikon A1R confocal microscope with CFI Plan Apo objectives running ×60 magnification was used for live-cell imaging. Multicolor images were acquired using lasers of 488, 561, and 647 nm. The microscope stage was equipped with a Chamlide TC system (Live Cell Instrument), which was used to maintain the temperature (37°C) and CO_2 concentration (10%).

For the JNK-KTR and ERK-KTR experiments and pS6 immunocytochemistry, neurons were starved in Ringer's solution (145 mM NaCl, 2.5 mM KCl, 10 mM glucose, 10 mM HEPES, 2 mM $CaCl_2$, and 1 mM $MgCl_2$) for 1 to 3 hours. For photoactivation, the 488-nm laser emitted through a Galvano scanner was incorporated in a hybrid confocal scan head with a high-speed selector (Nikon). For most of the in vitro experiments, we used a light intensity of 5 $\mu W/mm^2$ with a frequency of 1 s in every 3 min (duty cycle, 0.55%) for activation, unless otherwise specified. A laser intensity of 5 $\mu W/mm^2$ and a duration of 11 s in every 5 min were used for the local stimulation of HeLa cells. We adjusted the stimulation area based on information obtained using the Nikon imaging software (NIS-elements AR 64-bit version 4.10, Laboratory Imaging).

Light-emitting diode stimulation and cell viability assay

A TouchBright W-96 LED (light-emitting diode) Excitation System (Live Cell Instrument) was used for the light stimulation of HeLa cells and oligodendrocytes subjected to cell viability tests. By adjusting the power intensity of the LED system, we could illuminate cells with 470-nm light with 0 to 20 $\mu W/mm^2$. For most of the experiments, a light intensity of 5 $\mu W/mm^2$ and a duty cycle of 33% (light for 1 s followed by dark for 2 s) was used. For the induction of apoptosis in oligodendrocytes, light stimulation for 12 hours was performed.

To analyze the viability of cells in 96-well plates, we used a Cell Counting Kit-8 (catalog no. CK04-01, Dojindo Molecular Technologies). According to the manufacturer's instructions, light-stimulated cells were incubated in medium containing 10% Cell Counting Kit-8 solution, and the absorbance at 450 nm was measured using a VersaMax microplate reader (Molecular Devices).

Antibodies

The following antibodies with diluent factors were used in this study: chicken anti-GFP (1:1000; catalog no. A10262, Thermo Fisher Scientific), rabbit anti–phospho-S6 ribosomal protein (S235/S236) (1:500; catalog no. 4858, Cell Signaling Technology), rabbit anti–phospho-S6 ribosomal protein (S240/S244) (1:400; catalog no. 5364, Cell Signaling Technology), mouse anti–βIII-tubulin (1:500; catalog no. 4466, Cell Signaling Technology), rabbit anti–phospho-p44/42 MAPK (Erk1/2) (Thr^{202}/Tyr^{204}) (1:10,000; catalog no. 4370, Cell Signaling Technology), rabbit anti-SOX2 (1:100; catalog no. ab92494, Abcam), rabbit anti-DCX (1:400; catalog no. ab18723, Abcam), rabbit anti-calretinin (1:100; catalog no. ab702, Abcam), rabbit anti-Fas (1:100; catalog no. ab82419, Abcam), and rat anti-BrdU (1:100; catalog no. ab6326, Abcam).

Immunocytochemistry

For ICC staining, cells were fixed with 4% paraformaldehyde (PFA) in phosphate-buffered saline (PBS) for 20 min at room temperature and then washed three times with PBS. The cells were permeabilized with 0.2% Triton X-100 in PBS (PBS-X) for 10 min at room temperature, washed three times with 0.1% Tween 20 in PBS (PBS-T), and blocked with 10% FBS for 1 hour at room temperature. Primary antibodies were diluted in PBS-T and incubated with the cells for 12 to 16 hours at 4°C. The cells were then washed five times with PBS-T and incubated for 1 hour at room temperature with secondary antibodies diluted in 10% FBS. The cells were washed six times with PBS-T and stored in cold PBS until the imaging analysis was performed.

AAV and lentivirus production

AAVs were produced using the three-plasmid cotransfection system. Briefly, the transfer plasmid (containing the transgene-expressing cassette), packaging plasmid (pRC-DJ/8), and helper plasmid (pHelper) were diluted in Opti-MEM (catalog no. 31985-070, Gibco) at a ratio of 1:1:2. Polyethylenimine (PEI) was added to the solution to produce a 2.5:1 mixture of DNA (micrograms)/PEI (nanograms). Following a 15-min incubation at room temperature, the solution was distributed to 15-cm dishes on which HEK293T cells had been grown to 75 to 80% confluency. The culture medium was completely changed after 4 hours of transfection. At 60 to 72 hours after transfection, the cells were harvested and centrifuged at 3300*g* for 20 min at 4°C. The pellet was resuspended in 14 ml of lysis buffer [50 mM tris-Cl (pH 8.0), 150 mM NaCl, and 2 mM $MgCl_2$] and mixed with 10% sodium deoxycholate (final concentration, 0.5%) and benzonase (final concentration, 50 U/ml). Each lysate was incubated at 37°C for 30 min, subjected to three or four rounds of freeze and thaw, and centrifuged at 12,000*g* for 30 min at 4°C. The supernatant was loaded to an iodixanol gradient and subjected to ultracentrifugation at 69,000 rpm for 1 hour at 4°C. The 40% iodixanol fraction was extracted, washed four times with cold PBS in a 100,000 molecular weight cutoff Amicon tube, and concentrated by centrifugation at 3000*g* to achieve a volume of 150 to 200 μl.

For lentivirus production, the transfer plasmid, Δ8.9 plasmid, and vesicular stomatitis virus G (vsvg) plasmid were diluted in Opti-MEM at a ratio of 2:1.5:1. PEI was added to the solution to achieve a 2.5:1 mixture of DNA (micrograms)/PEI (nanograms). Transfection was performed as described for AAV. The culture supernatant was collected, centrifuged at 2000 rpm for 5 min at 4°C, and filtered. Ultracentrifugation at 25,000 rpm for 90 min at 4°C was used to obtain lentiviral concentrates, which were dissolved in cold PBS.

In vitro viral transduction

For the transduction of cultured neurons or oligodendrocytes using AAV, viral concentrates were dissolved in neuronal plating medium without HS or basal chemically defining medium. Half of the supernatant from each plate was mixed with fresh culture medium to produce a conditioned medium. The viral solution was then added to the plates and incubated at 37°C. After 24 hours, all of the medium was replaced with conditioned medium. A multiplicity of infection (MOI) of 5000 to 20,000 was used for transduction.

BDNF ELISA

Supernatants of cultured rat hippocampal neurons exposed to light stimulation were subjected to ELISA using a BDNF Rat ELISA kit (catalog no. ERBDNF, Invitrogen) according to the manufacturer's instructions. Briefly, the supernatants were diluted 10-fold, dispensed to the BDNF antigen–precoated plate, and incubated for 2.5 hours at room temperature. The plate was washed four times, treated with the biotinylated antibody, and incubated for 1 hour at room temperature. The samples were washed, incubated in the streptavidin–horseradish peroxidase (HRP) solution for 45 min, washed again, and incubated with trimethylboron substrate for 30 min at room temperature in the dark. Stop Solution was added to the wells, and absorbances at 450 and 550 nm were measured using a VersaMax microplate reader. A standard curve was generated by plotting the average absorbance (450 nm minus 550 nm) of the standard solution provided with the kit.

ERK-KTR analysis in cultured neurons

DIV 1 to DIV 2 neurons were transfected with CMV-ERK-KTR-FuRed. Starvation of the neurons was performed before the imaging experiment using Ringer solution for 1 hour. DIV 7 neurons were either transduced by AAV-CAG-optoFAS and light-stimulated for 4 hours or transduced by AAV-CAG-EGFP and treated with sFasL (100 ng/ml) to induce BDNF secretion. To concentrate the supernatant of the DIV 7 neurons, Amicon Ultra-15 Centrifugal Filter Unit (catalog no. UFC901096, Millipore) and Amicon Ultra-0.5 Centrifugal Filter Unit (catalog no. UFC501096, Millipore) were used. The concentrated supernatants were treated to the ERK-KTR sensor–expressing DIV 1 to DIV 2 neurons during the live imaging. Preincubation with 500 nM rapamycin was performed 12 hours before the experiment to block the mTOR pathway. Incubation with 10 μM ANA-12 was conducted during the starvation before the experiment.

Animals

C57BL/6 inbred mice were purchased from the Jackson Laboratory (JAX Mice and Services). Homozygous BDNF-floxed mice ($Bdnf^{tm3Jae}$/J) were obtained from the Jackson Laboratory and bred in the KAIST animal facility. 5XFAD mice (B6SJL-Tg(APPSwFlLon,PSEN1*M146L*L286V)6799Vas/Mmjax) were donated by I. Mook-Jung (Seoul National University). Mice were subjected to stereotactic surgery at the age of 8 weeks. All mice were given free access to food and water. All experimental procedures were performed in accordance with the guidelines of the Institutional Animal Care and Use Committee at KAIST.

Stereotactic viral injection and light stimulation

For stereotactic surgery, each mouse was anesthetized with Avertin (240 mg/kg; 2,2,2,-tribromoethanol, catalog no. T48402, Sigma-Aldrich) or a mixture of ketamine (120 mg/kg; Vspharm, Korea) and xylazine (10 mg/kg; Vspharm). Scalp hair was shaved and the surgical field was scrubbed with a 10% betadine solution. A heating pad (Live Cell Instrument) was used to maintain the mouse's body temperature. An incision was made on the scalp, and craniotomy was performed by drilling the skull (about 0.5 mm in diameter). A viral mixture (volume, 0.5 μl) was infused using a World Precision Instruments 33-gauge blunt NanoFil needle at a rate of 100 nl/min. The used viral titers were as follows: AAV-Nestin-Cre, 3×10^{11} genome copy (GC)/ml; AAV-hSyn-DIO-optoFAS, 5×10^{11} GC/ml; and AAV-hSyn-DIO-EGFP, 5×10^{11} GC/ml. The stereotactic coordinates used for the DG were AP-2.06, ML 1.18, and DV 1.7. An optic fiber of Ø 200 μm (Doric) was implanted 0.2 mm above the viral injection site at 1 week after the injection.

An optic fiber coupled with a blue diode 473-nm laser (MBL-III-473m, CNI) was used for in vivo delivery of blue light. Light stimulation of the mouse brain was performed at an intensity of 5 mW/mm^2

and a frequency of 500 mHz (33% duty cycle). For the repetitive stimulation experiments, the light was applied for 4 hours/day for 3 to 5 days.

Pharmacological treatment of animals

Intraperitoneal injection of rapamycin was performed in mice as described previously (*44*). Briefly, rapamycin (LC Labs) was dissolved in 100% ethanol to produce a stock solution (25 mg/ml) and stored at −80°C. For injection, the rapamycin was diluted to 10 mg/kg in PBS containing 5% polyethylene glycol 400 and 5% Tween 80. Vehicle solution was produced by replacing rapamycin with distilled water. For single light stimulation experiments, mice were subjected to four (twice a day for 2 days) intraperitoneal rapamycin injections before illumination. For repetitive stimulation experiments, rapamycin was administrated daily for 2 weeks.

ANA-12 (catalog no. 4781, Tocris) was intraperitoneally injected to mice as previously described (*45*). Briefly, a stock solution of ANA-12 dissolved in dimethyl sulfoxide (DMSO; 20 mM) was diluted in normal saline (0.9% NaCl) to produce a working solution. For the vehicle solution, 1% DMSO was used. ANA-12 (0.5 mg/kg) was delivered 3.5 hours before the initiation of light stimulation in all experiments.

For the administration of BrdU (catalog no. B9285, Sigma-Aldrich) to mice, BrdU was dissolved in normal saline to produce a solution (10 mg/ml). BrdU (100 mg/kg) was injected to the mouse peritoneum at the start of every round of light stimulation.

Intracerebroventricular injection of LPS (catalog no. L2880, Sigma-Aldrich) was performed as described previously (*46*). LPS (20 ng) was dissolved in PBS for a single injection. The brain was harvested 2 hours after this administration.

Immunohistochemistry

For conventional IHC staining, mice were transcardially perfused with cold PBS and fixed in 4% PFA for at least 12 hours at 4°C. Following fixation, brains were harvested, washed in cold PBS, and sectioned into 50-μm coronal slices using a VT1200S vibratome (Leica). The obtained slices were washed six times with 0.3% PBS-X. Blocking was performed using 5% normal goat serum (NGS; catalog no. ab7481, Abcam) dissolved in 0.3% PBS-X for 1.5 hours. The primary antibody was diluted in 0.3% PBS-X containing 5% NGS and applied to the sections for 12 to 16 hours at 4°C. The slices were washed six times with 0.3% PBS-X and incubated with secondary antibodies dissolved in 0.3% PBS-X containing 5% NGS for 1 hour at room temperature. The slices were washed six times with 0.3% PBS-X and mounted onto glass slides with VECTASHIELD Antifade Mounting Medium with 4′,6-diamidino-2-phenylindole (catalog no. H-1200, Vector Laboratories).

For BrdU staining, the sectioned slices were washed three times with PBS, incubated in 2 M HCl for 30 min at room temperature, incubated with 1 M sodium borate buffer for 10 min at room temperature, and immediately washed three times with PBS. The steps of blocking and incubation with the primary and secondary antibodies were identical to those described above for conventional IHC.

For staining of pErk, sectioned brain slices were incubated in 1% $NaBH_4$ solution for 15 min at room temperature, washed three times, and treated with 3% H_2O_2 solution in PBS containing 10% ethanol for 20 min at room temperature. The slices were washed twice with PBS, blocked in 0.3% PBS-X containing 5% NGS, incubated with pErk antibody for 36 hours at 4°C, and then washed six times with TNT buffer [0.1 M tris-HCl (pH 7.5), 0.15 M NaCl, and 0.05% Tween 20 dissolved in distilled water]. HRP was applied for 1 hour at room temperature. The slices were washed six times, incubated with TSA Cyanine 3 Tyramide Reagent (1:50; catalog no. SAT704A001EA, PerkinElmer) for 10 min, and immediately washed with TNT buffer. If needed, blocking and additional antibody treatments were performed as described for conventional IHC.

Quantitative real-time polymerase chain reaction

Cultured neurons were incubated in 12-well plates. AAVs were applied to the plates at MOI of 20,000. Following light stimulation or soluble Fas ligand treatment, the neurons were harvested, centrifuged, and stored at −80°C until RNA isolation was performed. Hippocampal tissue was dissected on ice with a razor immediately after light stimulation, in a darkroom. The harvested tissue was snap-frozen and stored at −80°C until RNA isolation was performed.

RNA was isolated and purified using a PureLink RNA Mini Kit (catalog no. 12183018A, Ambion) following the manufacturer's protocol. The obtained mRNA (1 μg) was used to produce cDNA with a SuperScript III First-Strand Synthesis System (catalog no. 18080-051, Invitrogen). qRT-PCR was performed using the Solg 2× Real-Time PCR Smart mix (catalog no. SRH72-M40h, SolGent) and EvaGreen dye. The manufacturer's recommended three-step cycling protocol was used for 50 cycles. The following primers were used: rat BDNF, 5′-GGTTCGAGAGGTCTGACGAC-3′ (forward) and 5′-CAAAGGCACTTGACTGCTGA-3′ (reverse); rat IGF-1, 5′-CCTGGGCTTTGTTTTCACTTCGG-3′ (forward) and 5′-TTTGTAGGCTTCAGCGGAGCAC-3′ (reverse); rat IL-6, 5′-CAGGAACGAAAGTCAACTCCA-3′ (forward) and 5′-ATCAGTCCCAAGAAGGCAACT-3′ (reverse); rat NeuroD, 5′-GTTCCACGTCAAGCCGCCGC-3′ (forward) and 5′-AGCGGCACCCGAGGAGAAGA-3′ (reverse); rat Hes5, 5′-CGGCACCAGCCCAACTCCAA-3′ (forward) and 5′-GGAACTGCACCGCCTCCTGC-3′ (reverse). Mouse BDNF I, 5′-CCTGCATCTGTTGGGGAGAC-3′ (forward) and 5′-CGCCTTCATGCAACCGAAGTAT-3′ (reverse); mouse BDNF II, 5′-ACCTTTTCCTCCTCCTGCG-3′ (forward) and 5′-TGGATGAAGTACTACCACCTCGG-3′ (reverse); mouse BDNF III, 5′-TGAGACTGCGCTCCACTCCC-3′ (forward) and 5′-CGCCTTCATGCAACCGAAGTAT-3′ (reverse); mouse BDNF IV, 5′-CAGAGCAGCTGCCTTGATGTTT-3′ (forward) and 5′-CGCCTTCATGCAACCGAAGTAT-3′ (reverse); mouse BDNF V, 5′-CTCTGTGTAGTTTCATTGTGTGTTC-3′ (forward) and 5′-GAAGTGTACAAGTCCGCGTCCTTA-3′ (reverse); mouse BDNF VI, 5′-ACAATGTGACTCCACTGCCGG-3′ (forward) and 5′-CGCCTTCATGCAACCGAAGTAT-3′ (reverse); mouse BDNF VII, 5′-ACTTACAGGTCCAAGGTCAACG-3′ (forward) and 5′-GGACAGAGGGTCGGATACAG-3′ (reverse); mouse BDNF VIII, 5′-ATGACTGTGCATCCCAGGAGAAA-3′ (forward) and 5′-CGCCTTCATGCAACCGAAGTAT-3′ (reverse); mouse BDNF IXa, 5′-CCCAAAGCTGCTAAAGCGGGAGGAAG-3′ (forward) and 5′-GAAGTGTACAAGTCCGCGTCCTTA-3′ (reverse); mouse total BDNF, 5′-TCGTTCCTTTCGAGTTAGCC-3′ (forward) and 5′-TTGGTAAACGGCACAAAAC-3′ (reverse).

Behavioral experiments

To physiologically induce BDNF secretion, mice were placed onto a Mouse RotaRod (Ugo Basile) and subjected to exercise for 1 hour. Spatial working memory, which is dependent on the hippocampus, was assessed by measuring spontaneous alteration performance during the Y-maze task. The Y-maze chamber was made of acrylic, with three arms 120° apart from each other. Each arm has 40 cm in length, 17 cm

in height, 4 cm in width (bottom), and 13 cm in width (top). Mice were placed at the end of one maze arm and allowed to freely explore through the maze for 15 min. From the recorded video, we analyzed the moving sequence and total entries of arms. An entry was considered to have occurred when the mouse's hindlimb was placed within the arm. The percentage of spontaneous alteration was calculated as the number of triads containing entries into all three arms/maximum possible alternations (the total number of arms entered − 2) × 100.

The open field test was performed in a 42 cm by 42 cm by 42 cm–sized chamber made of acrylic. Each mouse was placed at the center of the chamber and permitted to move freely for 30 min. By analyzing the video-recorded data using OptiMouse (*47*), we obtained the total distance traveled and the time spent in the central area (20 cm by 20 cm). As a detection parameter, we used algorithm 6 of the OptiMouse software to detect body position. The average speed was calculated by total distance/time. The anxiety index was calculated as follows: (total time − time spent in the central area)/time spent in the central area. All mice were handled for 10 min a day for 3 days before the behavioral tests.

Gene set enrichment analysis

Among the expression datasets for Alzheimer's disease (GSE84422), age- and race-matched hippocampal samples of patients with Alzheimer's disease and healthy control were selected for the analysis. Mild Alzheimer's disease group was defined as patients with CDR scores of 0.5 and 1 and a Braak neurofibrillary tangle score of no more than 3 (GSM2234477, GSM2234481, GSM 2234484, GSM 2234500, and GSM2234517; five samples). Severe Alzheimer's disease group was defined as with CDR scores of 3 to 5 (GSM2234475, GSM2234476, GSM2234498, GSM2234499, and GSM2234501; five samples). Healthy control groups involved individuals with a CDR score of 0 (GSM2234471, GSM2234472, GSM2234488, GSM2234489, GSM2234503; five samples). GSEA was performed using cloud version of GSEA, version 19.0.25 (https://cloud.genepattern.org) with default parameters (*48*). The gene signature of BIOCARTA_FAS_PATHWAY (M9503), CREIGHTON_AKT1_SIGNALING_VIA_MTOR_UP (M15377), and BIOCARTA_MAPK_PATHWAY (M13863) was used for the analysis. GSEA was run for mild Alzheimer's disease versus healthy control, mild Alzheimer's disease versus severe Alzheimer's disease, and severe Alzheimer's disease versus healthy control, separately.

Quantification and statistical analysis

All images were analyzed using Nikon imaging software (NIS-elements AR 64-bit version 4.10, Laboratory Imaging). To calculate the induced apoptotic rate, the number of cells showing morphological features of apoptosis (shrinkage or blebbing of the cytoplasm in the case of HeLa cells and astrocytes; fragmentation of axons and dendrites in the case of neurons) was counted from six randomly selected imaging fields for each experimental condition. In most images, to select a region of interest (ROI) in the imaging field, we used the "Automated ROI" function of the Nikon imaging software. For analysis of pS6 ICC, the soma of each neuron was selected according to the boundary of the βIII-tubulin signal, and the intensity of the stained signal was calculated. The normalized C/N ratio of the JNK-KTR and ERK-KTR sensor was measured using the "Time Measurement" tool of the imaging software. To calculate the number of $pS6^+$ and $pErk^+$ cells in the GCL and SGZ of the tissue sections, cells revealing fluorescent signals greater than 500 arbitrary units were selected and counted using the "Object Count" function of the software.

The number of $BrdU^+$ cells per DG was estimated as previously described (*49*, *50*). Every sixth immunostained brain slice (50 μm in thickness) was selected and counted for $BrdU^+$ cells in the SGZ and GCL. The sampling was conducted to cover the dorsal DG (−1.55 to −3.65 mm from bregma). The sum of the $BrdU^+$ cells was multiplied by six to calculate the estimated number of cells. To calculate the number of cells showing colocalization of BrdU and other markers (SOX2, DCX, or calretinin), the same strategy was used in costained sections.

Statistical analysis was conducted using GraphPad Prism 7.00 (GraphPad Software). All data were expressed as means ± SEM. Statistical significance was assessed by using *t* test or analysis of variance (ANOVA), followed by Tukey's or Fisher's least significant difference post hoc tests. In the figures, $^*P < 0.05$, $^{**}P < 0.01$, $^{***}P < 0.001$, and $^{****}P < 0.0001$.

SUPPLEMENTARY MATERIALS

Supplementary material for this article is available at http://advances.sciencemag.org/cgi/content/full/6/17/eaaz9691/DC1

View/request a protocol for this paper from *Bio-protocol*.

REFERENCES AND NOTES

1. J. E. Toettcher, O. D. Weiner, W. A. Lim, Using optogenetics to interrogate the dynamic control of signal transmission by the Ras/Erk module. *Cell* **155**, 1422–1434 (2013).
2. L. J. Bugaj, A. J. Sabnis, A. Mitchell, J. E. Garbarino, J. E. Toettcher, T. G. Bivona, W. A. Lim, Cancer mutations and targeted drugs can disrupt dynamic signal encoding by the Ras-Erk pathway. *Science* **361**, eaao3048 (2018).
3. H. Wajant, The Fas signaling pathway: More than a paradigm. *Science* **296**, 1635–1636 (2002).
4. N. S. Corsini, I. Sancho-Martinez, S. Laudenklos, D. Glagow, S. Kumar, E. Letellier, P. Koch, M. Teodorczyk, S. Kleber, S. Klussmann, B. Wiestler, O. Brüstle, W. Mueller, C. Gieffers, O. Hill, M. Thiemann, M. Seedorf, N. Gretz, R. Sprengel, T. Celikel, A. Martin-Villalba, The death receptor CD95 activates adult neural stem cells for working memory formation and brain repair. *Cell Stem Cell* **5**, 178–190 (2009).
5. A. Reich, C. Spering, J. B. Schulz, Death receptor Fas (CD95) signaling in the central nervous system: Tuning neuroplasticity? *Trends Neurosci.* **31**, 478–486 (2008).
6. C. Choi, E. N. Benveniste, Fas ligand/Fas system in the brain: Regulator of immune and apoptotic responses. *Brain Res. Brain Res. Rev.* **44**, 65–81 (2004).
7. C. P. Beier, M. Kolbl, D. Beier, C. Woertgen, U. Bogdahn, A. Brawanski, CD95/Fas mediates cognitive improvement after traumatic brain injury. *Cell Res.* **17**, 732–734 (2007).
8. J. Khuman, W. P. Meehan III, X. Zhu, J. Qiu, U. Hoffmann, J. Zhang, E. Giovannone, E. H. Lo, M. J. Whalen, Tumor necrosis factor alpha and Fas receptor contribute to cognitive deficits independent of cell death after concussive traumatic brain injury in mice. *J. Cereb. Blood Flow Metab.* **31**, 778–789 (2011).
9. K. Y. Chang, D. Woo, H. Jung, S. Lee, S. Kim, J. Won, T. Kyung, H. Park, N. Kim, H. W. Yang, J. Y. Park, E. M. Hwang, D. Kim, W. D. Heo, Light-inducible receptor tyrosine kinases that regulate neurotrophin signalling. *Nat. Commun.* **5**, 4057 (2014).
10. N. Kim, J. M. Kim, M. Lee, C. Y. Kim, K.-Y. Chang, W. D. Heo, Spatiotemporal control of fibroblast growth factor receptor signals by blue light. *Chem. Biol.* **21**, 903–912 (2014).
11. T. Kyung, S. Lee, J. E. Kim, T. Cho, H. Park, Y.-M. Jeong, D. Kim, A. Shin, S. Kim, J. Baek, J. Kim, N. Y. Kim, D. Woo, S. Chae, C.-H. Kim, H.-S. Shin, Y. M. Han, D. Kim, W. D. Heo, Optogenetic control of endogenous Ca^{2+} channels in vivo. *Nat. Biotechnol.* **33**, 1092–1096 (2015).
12. D. M. Spencer, P. J. Belshaw, L. Chen, S. N. Ho, F. Randazzo, G. R. Crabtree, S. L. Schreiber, Functional analysis of Fas signaling in vivo using synthetic inducers of dimerization. *Curr. Biol.* **6**, 839–847 (1996).
13. Y. Ding, J. Li, J. R. Enterina, Y. Shen, I. Zhang, P. H. Tewson, G. C. Mo, J. Zhang, A. M. Quinn, T. E. Hughes, D. Maysinger, S. C. Alford, Y. Zhang, R. E. Campbell, Ratiometric biosensors based on dimerization-dependent fluorescent protein exchange. *Nat. Methods* **12**, 195–198 (2015).
14. B. Tummers, D. R. Green, Caspase-8: Regulating life and death. *Immunol. Rev.* **277**, 76–89 (2017).
15. S. Regot, J. J. Hughey, B. T. Bajar, S. Carrasco, M. W. Covert, High-sensitivity measurements of multiple kinase activities in live single cells. *Cell* **157**, 1724–1734 (2014).
16. C. Anacker, V. M. Luna, G. S. Stevens, A. Millette, R. Shores, J. C. Jimenez, B. Chen, R. Hen, Hippocampal neurogenesis confers stress resilience by inhibiting the ventral dentate gyrus. *Nature* **559**, 98–102 (2018).

17. M. Wang, P. Roussos, A. McKenzie, X. Zhou, Y. Kajiwara, K. J. Brennand, G. C. De Luca, J. F. Crary, P. Casaccia, J. D. Buxbaum, M. Ehrlich, S. Gandy, A. Goate, P. Katsel, E. Schadt, V. Haroutunian, B. Zhang, Integrative network analysis of nineteen brain regions identifies molecular signatures and networks underlying selective regional vulnerability to Alzheimer's disease. *Genome Med.* **8**, 104 (2016).
18. V. Nieto-Estévez, C. Defterali, C. Vicario-Abejón, IGF-I: A key growth factor that regulates neurogenesis and synaptogenesis from embryonic to adult stages of the brain. *Front. Neurosci.* **10**, 52 (2016).
19. M. Sairanen, G. Lucas, P. Ernfors, M. Castrén, E. Castrén, Brain-derived neurotrophic factor and antidepressant drugs have different but coordinated effects on neuronal turnover, proliferation, and survival in the adult dentate gyrus. *J. Neurosci.* **25**, 1089–1094 (2005).
20. M. A. Storer, D. Gallagher, M. P. Fatt, J. V. Simonetta, D. R. Kaplan, F. D. Miller, Interleukin-6 regulates adult neural stem cell numbers during normal and abnormal post-natal development. *Stem Cell Rep.* **10**, 1464–1480 (2018).
21. M. T. Jeon, J. H. Nam, W. H. Shin, E. Leem, K. H. Jeong, U. J. Jung, Y. S. Bae, Y. H. Jin, N. Kholodilov, R. E. Burke, S. G. Lee, B. K. Jin, S. R. Kim, In vivo AAV1 transduction with hRheb(S16H) protects hippocampal neurons by BDNF production. *Mol. Ther.* **23**, 445–455 (2015).
22. G. Baj, E. Leone, M. V. Chao, E. Tongiorgi, Spatial segregation of BDNF transcripts enables BDNF to differentially shape distinct dendritic compartments. *Proc. Natl. Acad. Sci. U.S.A.* **108**, 16813–16818 (2011).
23. T. Sasaki, V. C. Piatti, E. Hwaun, S. Ahmadi, J. E. Lisman, S. Leutgeb, J. K. Leutgeb, Dentate network activity is necessary for spatial working memory by supporting CA3 sharp-wave ripple generation and prospective firing of CA3 neurons. *Nat. Neurosci.* **21**, 258–269 (2018).
24. K. M. Tye, K. Deisseroth, Optogenetic investigation of neural circuits underlying brain disease in animal models. *Nat. Rev. Neurosci.* **13**, 251–266 (2012).
25. L. E. Fielmich, R. Schmidt, D. J. Dickinson, B. Goldstein, A. Akhmanova, S. van den Heuvel, Optogenetic dissection of mitotic spindle positioning in vivo. *eLife* **7**, e38198 (2018).
26. J. M. Kim, M. Lee, N. Kim, W. D. Heo, Optogenetic toolkit reveals the role of Ca^{2+} sparklets in coordinated cell migration. *Proc. Natl. Acad. Sci. U.S.A.* **113**, 5952–5957 (2016).
27. M. Z. Wilson, P. T. Ravindran, W. A. Lim, J. E. Toettcher, Tracing information flow from Erk to target gene induction reveals mechanisms of dynamic and combinatorial control. *Mol. Cell* **67**, 757–769.e5 (2017).
28. S. M. Jones, A. Kazlauskas, Growth-factor-dependent mitogenesis requires two distinct phases of signalling. *Nat. Cell Biol.* **3**, 165–172 (2001).
29. F. Li, N. Omori, G. Jin, S. J. Wang, K. Sato, I. Nagano, M. Shoji, K. Abe, Cooperative expression of survival p-ERK and p-Akt signals in rat brain neurons after transient MCAO. *Brain Res.* **962**, 21–26 (2003).
30. Y. Li, Z. Peng, B. Xiao, C. R. Houser, Activation of ERK by spontaneous seizures in neural progenitors of the dentate gyrus in a mouse model of epilepsy. *Exp. Neurol.* **224**, 133–145 (2010).
31. Z. Tan, J. Levid, S. S. Schreiber, Increased expression of Fas (CD95/APO-1) in adult rat brain after kainate-induced seizures. *Neuroreport* **12**, 1979–1982 (2001).
32. M. Perovic, V. Tesic, A. Mladenovic Djordjevic, K. Smiljanic, N. Loncarevic-Vasiljkovic, S. Ruzdijic, S. Kanazir, BDNF transcripts, proBDNF and proNGF, in the cortex and hippocampus throughout the life span of the rat. *Age* **35**, 2057–2070 (2013).
33. W. Singer, M. Manthey, R. Panford-Walsh, L. Matt, H.-S. Geisler, E. Passeri, G. Baj, E. Tongiorgi, G. Leal, C. B. Duarte, I. L. Salazar, P. Eckert, K. Rohbock, J. Hu, J. Strotmann, P. Ruth, U. Zimmermann, L. Rüttiger, T. Ott, T. Schimmang, M. Knipper, BDNF-live-exon-visualization (BLEV) allows differential detection of BDNF transcripts in vitro and in vivo. *Front Mol. Neurosci.* **11**, 325 (2018).
34. J. C. Knight, E. L. Scharf, Y. Mao-Draayer, Fas activation increases neural progenitor cell survival. *J. Neurosci. Res.* **88**, 746–757 (2010).
35. J. Knight, C. Hackett, J. Solty, Y. Mao-Draayer, Fas receptor modulates lineage commitment and stemness of mouse neural stem cells. *Neurosci. Med.* **2**, 132–141 (2011).
36. S. Nagata, Mutations in the Fas antigen gene in lpr mice. *Semin. Immunol.* **6**, 3–8 (1994).
37. M. Blurton-Jones, M. Kitazawa, H. Martinez-Coria, N. A. Castello, F. J. Müller, J. F. Loring, T. R. Yamasaki, W. W. Poon, K. N. Green, F. M. LaFerla, Neural stem cells improve cognition via BDNF in a transgenic model of Alzheimer disease. *Proc. Natl. Acad. Sci. U.S.A.* **106**, 13594–13599 (2009).
38. O. Lindvall, Z. Kokaia, Neurogenesis following stroke affecting the adult brain. *Cold Spring Harb. Perspect. Biol.* **7**, a019034 (2015).
39. K. Jin, A. L. Peel, X. O. Mao, L. Xie, B. A. Cottrell, D. C. Henshall, D. A. Greenberg, Increased hippocampal neurogenesis in Alzheimer's disease. *Proc. Natl. Acad. Sci. U.S.A.* **101**, 343–347 (2004).
40. E. P. Moreno-Jimeénez, M. Flor-García, J. Terreros-Roncal, A. Rabano, F. Cafini, N. Pallas-Bazarra, J. Ávila, M. Llorens-Martín, Adult hippocampal neurogenesis is abundant in neurologically healthy subjects and drops sharply in patients with Alzheimer's disease. *Nat. Med.* **25**, 554–560 (2019).
41. K. Stavitsky, A. M. Brickman, N. Scarmeas, R. L. Torgan, M. X. Tang, M. Albert, J. Brandt, D. Blacker, Y. Stern, The progression of cognition, psychiatric symptoms, and functional abilities in dementia with Lewy bodies and Alzheimer disease. *Arch. Neurol.* **63**, 1450–1456 (2006).
42. W. Maetzler, I. Liepelt, D. Berg, Progression of Parkinson's disease in the clinical phase: Potential markers. *Lancet Neurol.* **8**, 1158–1171 (2009).
43. Y. Chen, V. Balasubramaniyan, J. Peng, E. C. Hurlock, M. Tallquist, J. Li, Q. R. Lu, Isolation and culture of rat and mouse oligodendrocyte precursor cells. *Nat. Protoc.* **2**, 1044–1051 (2007).
44. S. M. Park, J. S. Lim, S. Ramakrishina, S. H. Kim, W. K. Kim, J. Lee, H. C. Kang, J. F. Reiter, D. S. Kim, H. H. Kim, J. H. Lee, Brain somatic mutations in MTOR disrupt neuronal ciliogenesis, leading to focal cortical dyslamination. *Neuron* **99**, 83–97.e7 (2018).
45. Q. Ren, M. Ma, C. Yang, J.-C. Zhang, W. Yao, K. Hashimoto, BDNF-TrkB signaling in the nucleus accumbens shell of mice has key role in methamphetamine withdrawal symptoms. *Transl. Psychiatry* **5**, e666 (2015).
46. M. A. Lawson, J. M. Parrott, R. H. McCusker, R. Dantzer, K. W. Kelley, J. C. O'Connor, Intracerebroventricular administration of lipopolysaccharide induces indoleamine-2,3-dioxygenase-dependent depression-like behaviors. *J. Neuroinflammation* **10**, 87 (2013).
47. Y. Ben-Shaul, OptiMouse: A comprehensive open source program for reliable detection and analysis of mouse body and nose positions. *BMC Biol.* **15**, 41 (2017).
48. A. Subramanian, P. Tamayo, V. K. Mootha, S. Mukherjee, B. L. Ebert, M. A. Gillette, A. Paulovich, S. L. Pomeroy, T. R. Golub, E. S. Lander, J. P. Mesirov, Gene set enrichment analysis: A knowledge-based approach for interpreting genome-wide expression profiles. *Proc. Natl. Acad. Sci. U.S.A.* **102**, 15545–15550 (2005).
49. S. H. Choi, E. Bylykbashi, Z. K. Chatila, S. W. Lee, B. Pulli, G. D. Clemenson, E. Kim, A. Rompala, M. K. Oram, C. Asselin, J. Aronson, C. Zhang, S. J. Miller, A. Lesinski, J. W. Chen, D. Y. Kim, H. van Praag, B. M. Spiegelman, F. H. Gage, R. E. Tanzi, Combined adult neurogenesis and BDNF mimic exercise effects on cognition in an Alzheimer's mouse model. *Science* **361**, eaan8821 (2018).
50. T. Kitamura, Y. Saitoh, N. Takashima, A. Murayama, Y. Niibori, H. Ageta, M. Sekiguchi, H. Sugiyama, K. Inokuchi, Adult neurogenesis modulates the hippocampus-dependent period of associative fear memory. *Cell* **139**, 814–827 (2009).

Acknowledgments: We thank J. Shin for experimental support, S. Lee and H. Jung for helpful discussions, M. Klugmann for providing the AAV-MAG-EGFP vector, and I. Mook-Jung for providing the 5XFAD mice. **Funding:** This work was supported by the Institute for Basic Science (no. IBS-R001-D1) and the KAIST Institute for the BioCentury and the National Research Foundation of Korea (NRF) grant funded by the Ministry of Science and ICT (MSIT) (2020R1A2C3014742), Republic of Korea. **Author contributions:** Seokhwi Kim, N.K., and W.D.H. conceived the idea and designed the experiments. Seokhwi Kim performed and analyzed all experiments. J.L. contributed to the analysis of the behavioral experiments. All authors contributed to the data interpretations and discussions. Seokhwi Kim, N.K., and W.D.H. wrote the manuscript. **Competing interests:** The authors declare that they have no competing interests. **Data and materials availability:** All data needed to evaluate the conclusions in the paper are present in the paper and/or the Supplementary Materials. Additional data related to this paper may be requested from the authors.

Submitted 24 October 2019
Accepted 31 January 2020
Published 22 April 2020
10.1126/sciadv.aaz9691

Citation: S. Kim, N. Kim, J. Lee, S. Kim, J. Hong, S. Son, W. Do Heo, Dynamic Fas signaling network regulates neural stem cell proliferation and memory enhancement. *Sci. Adv.* **6**, eaaz9691 (2020).